Tesla-Report 2000-31

Beam Loss Monitors for TESLA

by

A. Batalov[0], K. Wittenburg[1]

[0] Institute For High Energy Physics IHEP, Protvino, Moskau
[1] Deutsches Elektronen Synchrotron DESY, D-22607 Hamburg,

16. November 2000

1 Introduction

The conceptual design of the electron-positron linear collider TESLA is described in Ref. 1. TESLA uses superconducting acceleration structures with high gradients and superconducting quadrupoles inside the same cryostat. Both components have a certain risk of beam loss induced quenches. Experiences from Tevatron and HERA shows, that an energy deposition of about 1 mJ/cm^3 within 20 ms in the superconductor of the quadrupole may result in a quench if the quadrupole is powered close to its critical current. About 5 mJ/cm^3 may quench it at half of this current and 10 mJ/cm^3 at 0 current (Ref. 2). An energy deposition of about 20 mJ/cm^3 may be critical for the superconducting cavity at gradients of 25 MV/m (Ref. 3). A beam loss monitor (BLM) system should detect loss rates before a critical energy deposition due to losses is reached. It should give a warning- or a fast beam-abort-signal in case of too intense beam losses.

A sensitive BLM system will be most helpful in setting-up and operating the accelerator even at low beam currents and with a small number of bunches to reach 100% transmission through the LINAC. Beam loss induced radiation will reduce the lifetime of electronic components in the TESLA tunnel. BLMs should measure the quantity and the position of losses to help the operator to reduce the radiation and to set up the beam parameters properly. This is true not only for the main Linac, but also for the beam delivery system of TESLA or other parts of the accelerator complex.

A spatial resolution of the distance of each quadrupole will be adequate, because the first indication of beam losses will happen inside the quadrupoles. This is especially true for the long parts of TESLA where no collimators will shield the components against failures. Collimators will need special loss monitors, which are not subject of this report.

In this report, the radiation levels of beam losses and background were calculated by Monte Carlo studies (Chap. 2). The sensitivity of BLM systems is calculated based on these results in Chap. 3.

Another source of radiation results from the dark current of the cavities. Electrons created on the inner surface of the cavity by field emission are accelerated towards the next quadrupole. Their energy can exceed several hundred MeV, depending on the module length and the position of creation. A significant number will be lost inside the quadrupole because of the non-matched magnetic field. The impact on the BLM system due to this radiation is discussed in appendix 1.

2 Monte Carlo Calculations

2.1 Material Geometry

The Monte Carlo Program Geant Version 3.2170 was used to simulate beam and dark current losses around the superconducting quadrupole of a Linac module. Fig. 1, 2 show the longitudinal and radial geometry of the quadrupole and the surrounding parts.

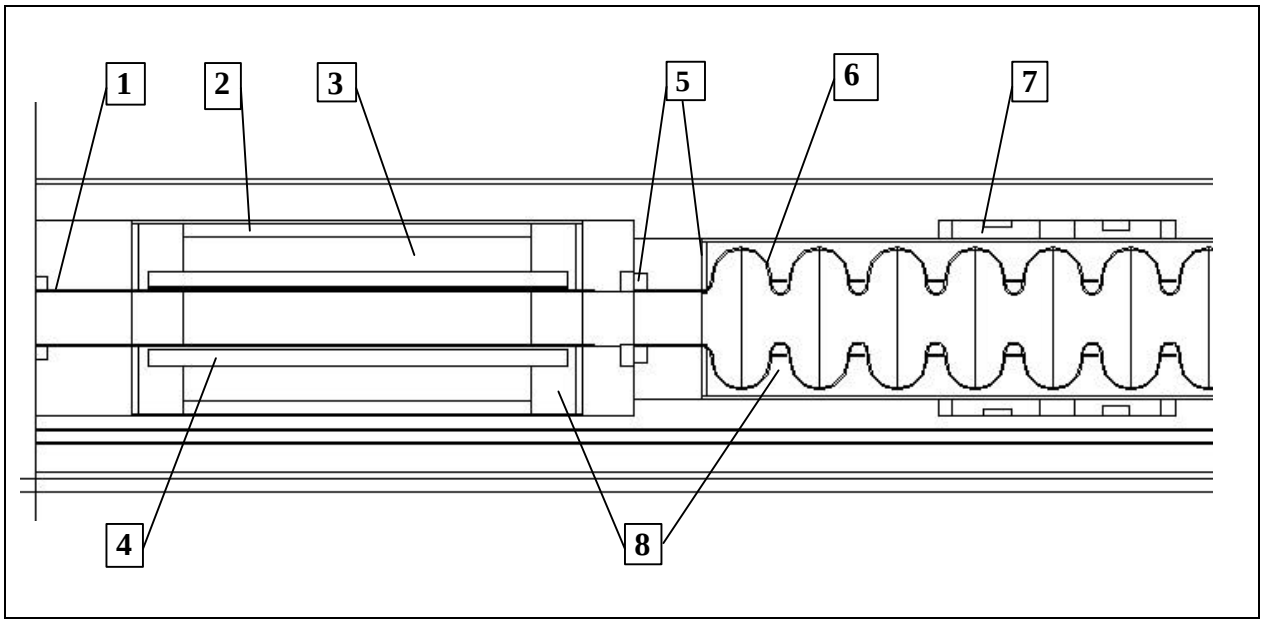

Fig. 1: Longitudinal geometry of the beam pipe with superconducting quadrupole, RF cavity and the adjacent parts. The beam enters from the right.

1. **Stainless steel beam pipe, flanges, quadrupole vessel.**
2. **Aluminum compression ring**
3. **Iron yoke.**
4. **Superconducting wires. 1.8 Cu : 1 (50%Nb + 50%Ti), packaging density is equal to 70%.**
5. **50%Nb + 50%Ti. Flanges and Cavity vessel faces.**
6. **Pure Niobium. Cavity.**
7. **Pure Titanium. Cavity vessel and cavity tuning system.**
8. **Liquid helium.**

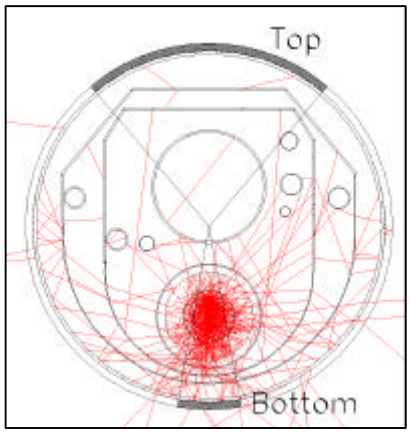

a)

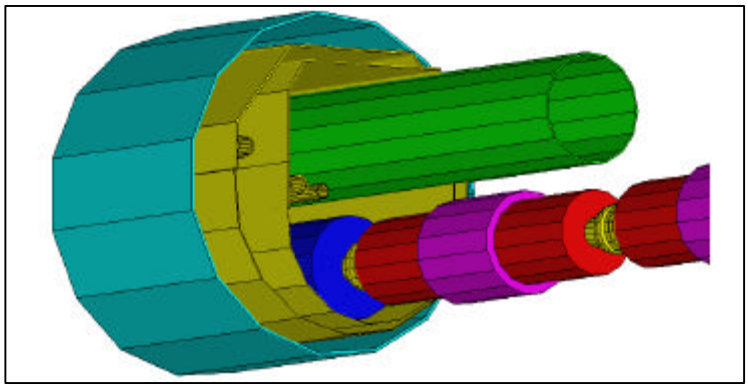

b)

Fig. 2: a) Radial geometry, front view. The shower after 25GeV electron loss is shown (e+, e- only). "Top" (azimuth angle 50^0 <F < 130^0), and "Bottom" (azimuth angle -80^0 <F < -100^0) zones are presented. b) 3 D view of cryostat in simulation. The He-Transfer-Leitung is located above the beam pipe.

2.2 Shower simmulations

Three different quantities of the shower outside of the cryostat were recorded: 1) the number of charged particles / cm^2 leaving the surface, 2) the energy deposition in 1 liter of air and 3) the

energy deposition in a 300 μm thick layer of silicon.The mean value over the bottom and top zones were calculated for better statistics and normalized to 1 cm^2 or 1 liter.
Unless otherwise noted, for the initial conditions a point-like lossof 200GeV electrons, in the middle of the quadrupole, with an angle of incidence of 0.2mrad at the upper part of the beam pipe, was assumed. The magnetic field of the quadrupole was roughly matched to the energy of the main beam (26.6T/m for 200GeV). The length of the quadrupole yoke is assumed to be 51.6 cm. 500 number of lost electrons where taken for each calculated value.

2.3 Results

Some dependencies of the results are tabled in the following, e.g. 2.3.1 Geometric dependence, 2.3.2 Energy dependence, 2.3.3 Incident-angle dependence and 2.3.4 Longitudinal point of loss. The main parameters in the tables are:

- The position of lost electrons is up – the beam was directed to the upper point of beam pipe.
- "Energy": Energy of lost electron in GeV,
- "Field" – quadrupole field gradient in T/m,
- Field(T/m) = 0.198 · E(GeV) in energy range from 5 to 125GeV,
  = 0.133 · E(GeV) in energy range from 125 to 400GeV.
- "Position": The position of the maximum relative to the point of losses in cm,
- "Width": The Full Width at Half Maximum in cm,
- "Counts": The number of charged particles (e+-) per lost electron per cm^2, other charged particles do not play any role.
- "Dep. energy Si": The deposited energy in a 300 μm Silicon layer per lost electron in [MeV/g/e^-]. The deposited energy in block of 300 microns x 1cm^2 of Si can be obtained from formula:
  E = Value (MeV/g/ e^-) · density(g/cm3) · area(cm2) · thickness(cm) = Value · 2.33 · 1 · 0.03
- "Dep. energy Air": The deposited energy in one liter of air in [MeV/liter/e^-]

The statistical errors for all results are less than 10%. The energy cuts in the simulations were 3 MeV for gammas and 1 MeV for electrons.

2.3.1 Geometric dependence

One can observe in Fig. 3 the azimuthal dependence in the results due to the asymmetry of the cryostat. The intensity of the shower is largest at the bottom zone of the cryostat because of the small distance and less material between the beam and the cryostat. There is a strong dependence on the azimuthal position of the loss in the beam pipe for high-energy electrons with the strong quadrupole field (Fig. 3a) because the strong magnetic field inside the quadrupole influences the shower expansion. It nearly vanished for weak quadrupole field (Fig. 3b).
The longitudinal distribution of the shower for beam energy of 200 GeV is shown in Fig. 4a and 4b. The distributions can be fitted by a shifted Gamma distribution (see Fig. 5):

$$x=z+P;\ f(x, l,k)=C\times x^{k-1}\times l^{k}\times e^{-lx}/G(k)$$

In the following, the position of the maximum is given by $P+(k-1)/l$ in cm relative to the point of loss while the FWHM is the Full Width AT Half Maximum in cm.

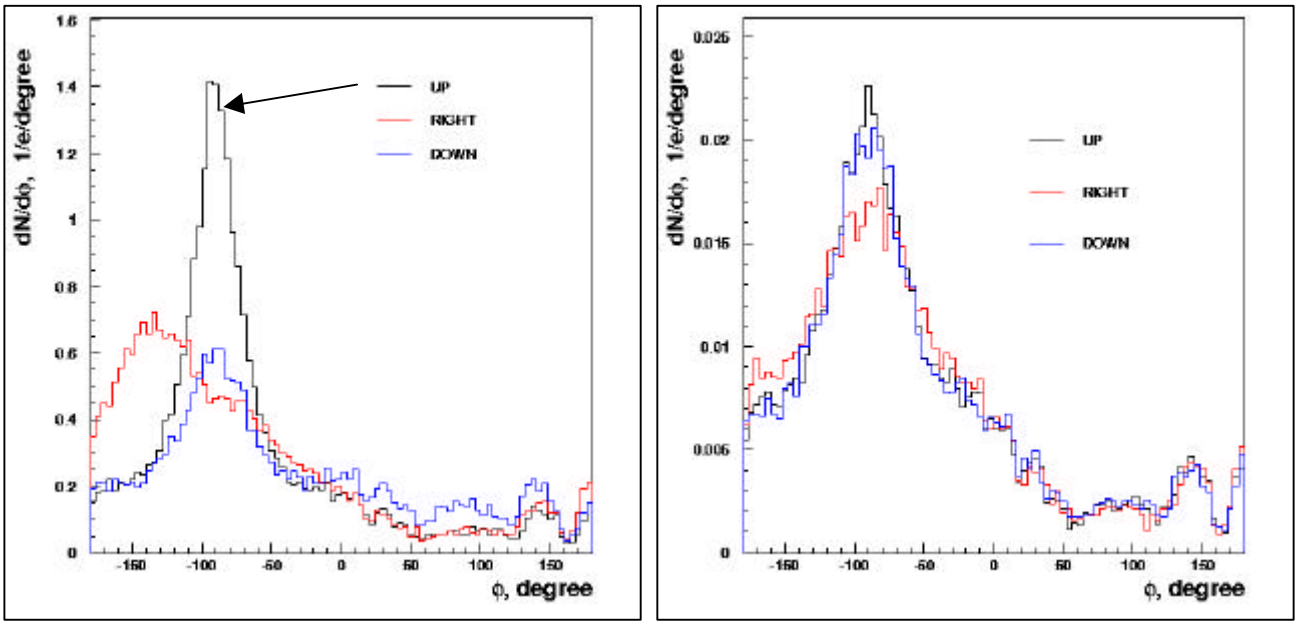

a) **b)**

Fig. 3: Azimuthal distribution of charged particles on the surface of vacuum vessel. a) The 200 GeV beam (field gradient 26.6T/m in Y focusing quadrupole) was directed: UP – to the upper point of beam pipe, DOWN – to the lower point of beam pipe, RIGHT – to the right point of beam pipe. The same for 5GeV beam (field 1T/m) is presented on figure b).

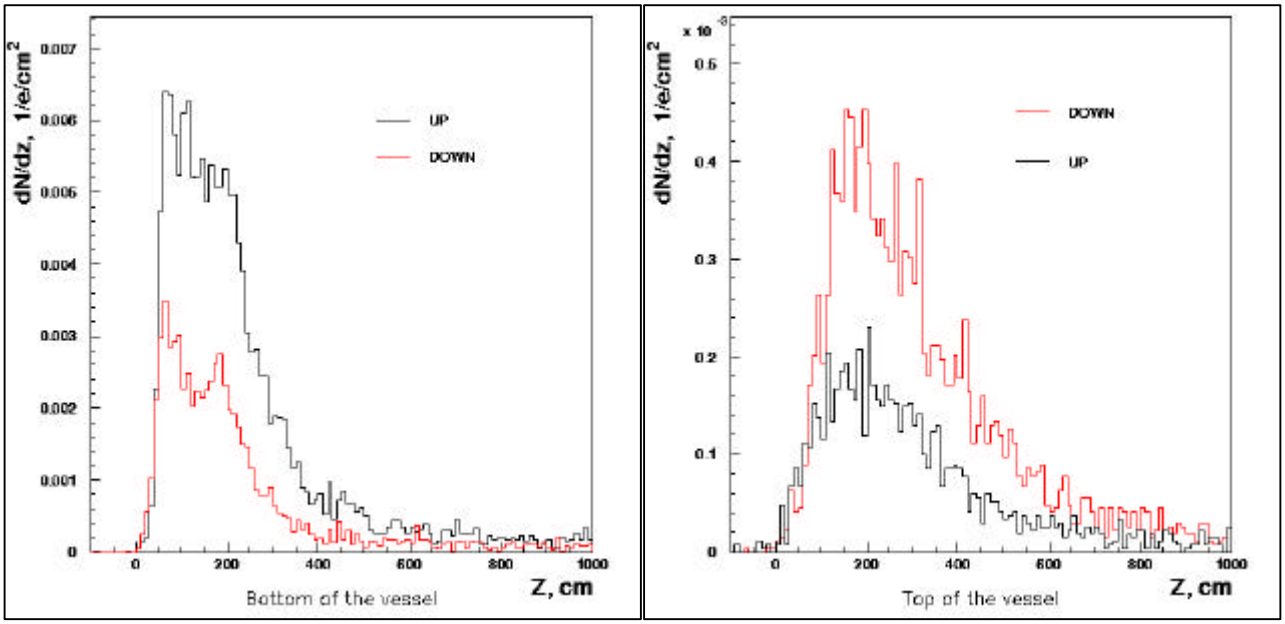

a) **b)**

Fig 4: Z distribution of the shower on the surface of the cryostat for 200GeV electrons (high quadrupole gradient) with losses directed in the "up" and "down" direction. a) Bottom zone of the vessel. b) top zone of the vessel.

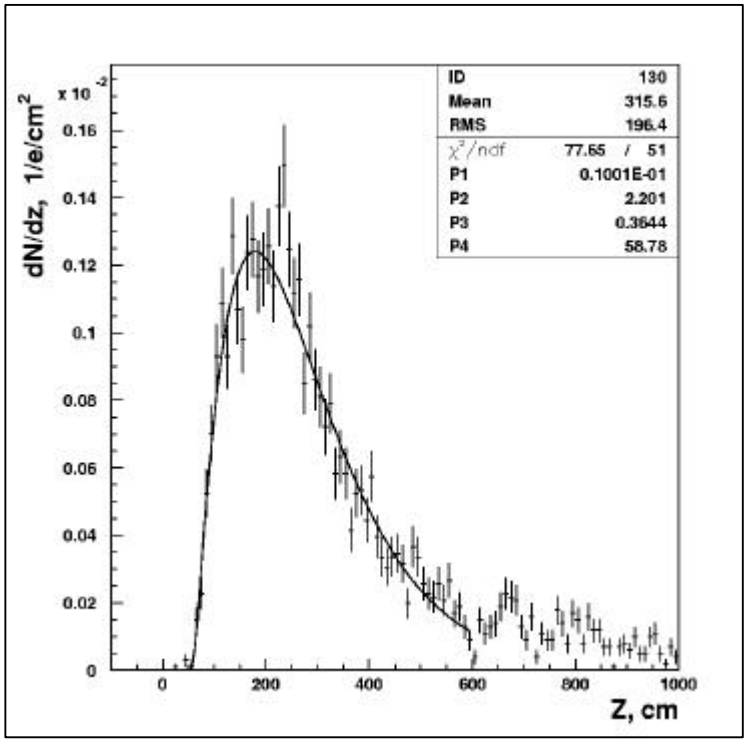

Fig. 5: Fit of the longitudinal shower distribution (solid line)

2.3.2 Energy dependence

Losses along the LINAC have been studied with Monte Carlo simulations for energies of the primary electron between 5 GeV and 400 GeV (see Tab. 1a,b). The energy dependence at top zone is linear with an error of less than 10 % (see Fig. 6 b). The same dependence for the bottom zone of the cryostat is not linear (see Fig. 6a) because of the quadrupole field. The magnetic field of the quadrupole turns the secondary electrons to the contrary wall of beam pipe i.e. to the bottom zone of cryostat. The difference between the top and bottom zone of cryostat is increasing from a factor about 10 for 5GeV to nearly 100 for high energy.

a)

Energy [GeV]	Field [T/m]	Position of Max [cm]	Width [cm]	Counts [/e/cm^2]	Dep. energy Si [MeV/g/ e$^-$]	Dep. energy Air [MeV/liter/ e$^-$]
5	1	178	205	$8.3\cdot10^{-5}$	$4.9\cdot10^{-4}$	$3.2\cdot10^{-4}$
25	5	167	251	$3.9\cdot10^{-4}$	$2.4\cdot10^{-3}$	$1.7\cdot10^{-3}$
50	10	173	226	$8.9\cdot10^{-4}$	$5.1\cdot10^{-3}$	$3.6\cdot10^{-3}$
100	19.8	115	208	$2.5\cdot10^{-3}$	$1.6\cdot10^{-2}$	$1.1\cdot10^{-2}$
125	24.8	110	197	$3.7\cdot10^{-3}$	$2.3\cdot10^{-2}$	$1.6\cdot10^{-2}$
125	16.6	113	208	$2.9\cdot10^{-3}$	$1.7\cdot10^{-2}$	$1.2\cdot10^{-2}$
150	20	116	213	$3.8\cdot10^{-3}$	$2.4\cdot10^{-2}$	$1.6\cdot10^{-2}$
200	26.6	106	195	$6.3\cdot10^{-3}$	$3.8\cdot10^{-2}$	$2.7\cdot10^{-2}$
250	33.3	100	180	$1.0\cdot10^{-2}$	$6.2\cdot10^{-2}$	$4.8\cdot10^{-2}$
400	53.2	78	140	$2.7\cdot10^{-2}$	$1.7\cdot10^{-1}$	$1.3\cdot10^{-1}$

b)

Energy [GeV]	Field [T/m]	Position of Max [cm]	Width [cm]	Counts [/e/cm^2]	Dep. energy Si [MeV/g/ e$^-$]	Dep. energy Air [MeV/liter/ e$^-$]
5	1	236	264	$7.2\cdot10^{-6}$	$3.5\cdot10^{-5}$	$2.7\cdot10^{-5}$
25	5	233	279	$3.0\cdot10^{-5}$	$1.6\cdot10^{-4}$	$1.3\cdot10^{-4}$
50	10	226	299	$5.2\cdot10^{-5}$	$3.1\cdot10^{-4}$	$2.4\cdot10^{-4}$
100	19.8	171	317	$9.3\cdot10^{-5}$	$4.1\cdot10^{-4}$	$3.3\cdot10^{-4}$
125	24.8	182	308	$1.1\cdot10^{-4}$	$5.8\cdot10^{-4}$	$4.2\cdot10^{-4}$
125	16.6	172	297	$1.3\cdot10^{-4}$	$5.5\cdot10^{-4}$	$4.7\cdot10^{-4}$
150	20	168	304	$1.5\cdot10^{-4}$	$7.6\cdot10^{-4}$	$5.2\cdot10^{-4}$
200	26.6	171	311	$1.7\cdot10^{-4}$	$9.8\cdot10^{-4}$	$6.9\cdot10^{-4}$
250	33.3	165	282	$2.5\cdot10^{-4}$	$1.2\cdot10^{-3}$	$9.2\cdot10^{-4}$
400	53.2	164	281	$3.8\cdot10^{-4}$	$1.6\cdot10^{-3}$	$1.5\cdot10^{-3}$

Tab. 1: Shower dependence from the energy of the lost electron; a) bottom b) top of the cryostat.

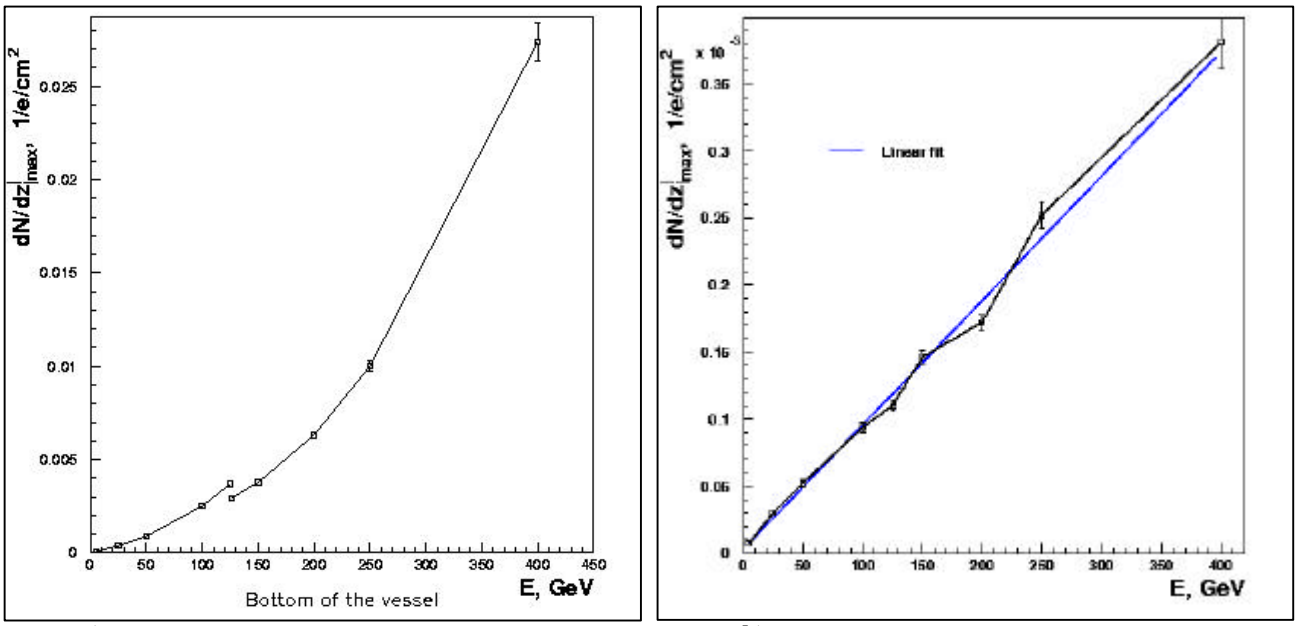

a) **b)**

Fig. 6: a) Dependence of the counts on the beam energy at the bottom of the cryostat.
b) Energy dependence at the top of the cryostat. Fit=$2.87\times10^{-6}(\pm3.4\times10^{-7})+9.27\times10^{-7}(\pm1.5\times10^{-8})\times E$

The situation is reversed for the down position of lost electrons.The beam energy dependence of the number of charged particles at bottom zone from the energy is linear, while the dependence for top zone of the cryostat is not linear. However, the non-linearity became important for energies above 250 GeV. Below this energy only small difference between up and down position of losses can be observed and the difference of the resulting shower between the top and bottom of the vessel is always about a factor 10.

2.3.3 Incident-angle dependence

The lost electrons hit the vacuum chamber at very small angles. The largest incident angle Θ is roughly the diameter of the beam pipe D divided by the maximum distance of the quadrupoles L, $\Theta \leq D/L \approx 1.7$ mrad. The following results were calculated with point-losses with energy of 200GeV in the upper part of the beam pipe at incident angles between 0 and 2mrad:

a)

incident angle [mrad]	Position [cm]	Width [cm]	Counts [/e/cm^2]	Dep. energy Si [MeV/g/ e$^-$]	Dep. energy Air [MeV/liter/ e$^-$]
0	169	275	$3.5\cdot10^{-3}$	$2.2\cdot10^{-2}$	$1.6\cdot10^{-2}$
0.002	169	267	$3.7\cdot10^{-3}$	$2.3\cdot10^{-2}$	$1.6\cdot10^{-2}$
0.01	142	271	$3.8\cdot10^{-3}$	$2.4\cdot10^{-2}$	$1.7\cdot10^{-2}$
0.1	112	214	$5.4\cdot10^{-3}$	$3.2\cdot10^{-2}$	$2.5\cdot10^{-2}$
0.2	107	195	$6.3\cdot10^{-3}$	$3.8\cdot10^{-2}$	$2.7\cdot10^{-2}$
1	93	162	$7.6\cdot10^{-3}$	$4.6\cdot10^{-2}$	$3.7\cdot10^{-2}$
2	84	146	$7.1\cdot10^{-3}$	$4.4\cdot10^{-2}$	$2.9\cdot10^{-2}$

b)

incident angle [mrad]	Position [cm]	Width [cm]	Counts [/e/cm^2]	Dep. energy Si [MeV/g/ e$^-$]	Dep. energy Air [MeV/liter/ e$^-$]
0	258	288	$3.2\cdot10^{-4}$	$1.6\cdot10^{-3}$	$1.2\cdot10^{-3}$
0.002	253	287	$3.1\cdot10^{-4}$	$1.6\cdot10^{-3}$	$1.1\cdot10^{-3}$
0.01	259	287	$2.9\cdot10^{-4}$	$1.5\cdot10^{-3}$	$1.1\cdot10^{-3}$
0.1	203	299	$2.1\cdot10^{-4}$	$1.1\cdot10^{-3}$	$7.7\cdot10^{-4}$
0.2	171	311	$1.7\cdot10^{-4}$	$9.8\cdot10^{-4}$	$6.9\cdot10^{-4}$
1	146	273	$1.7\cdot10^{-4}$	$8.8\cdot10^{-4}$	$6.6\cdot10^{-4}$
2	125	232	$1.8\cdot10^{-4}$	$9.8\cdot10^{-4}$	$7.0\cdot10^{-4}$

Table 2: Dependence on the incident angle of the lost electron at 200GeV; a) bottom of the cryostat; b) top of cryostat;

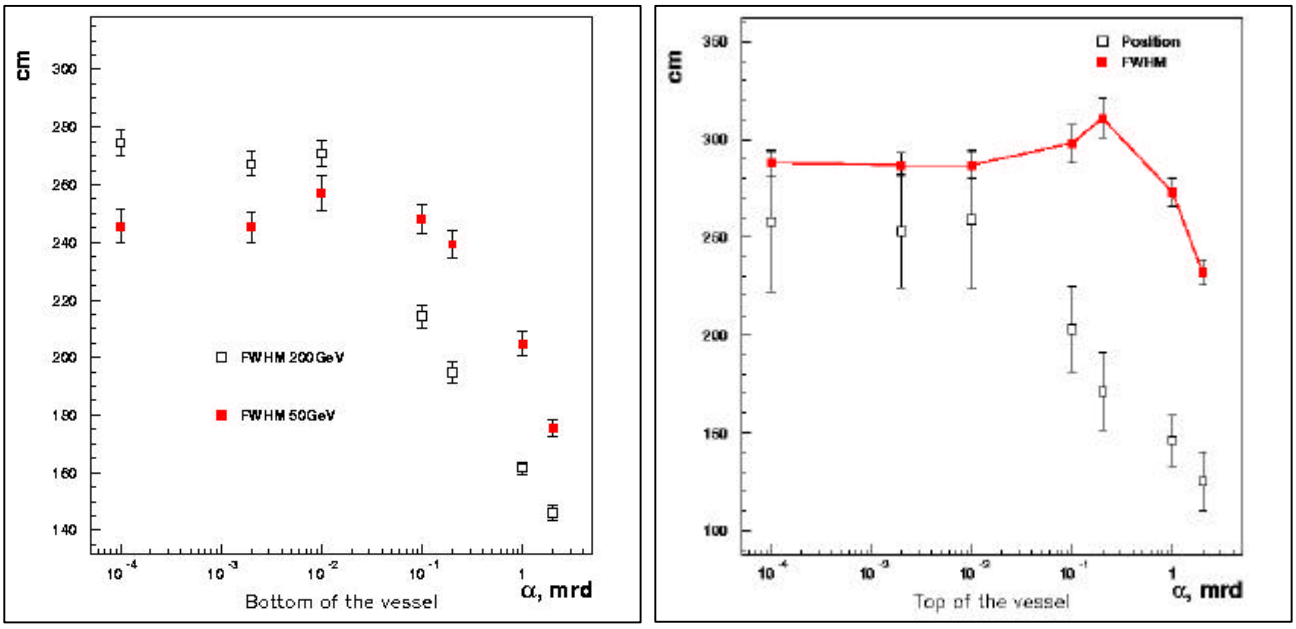

a) **b)**

Figure 7. a) FWHM versus incident angle at 50 and 200 GeV at the bottom of the vessel. b) Position and FWHM vs. incident angle at 200 GeV at the top of the vessel.

Table 2 and Fig. 7a, b show that the position variation of the maximum is much smaller than the width of the distribution for the interesting range between 0.1mrad and 2 mrad for 50 and 200 GeV. The resulting signal variation is in the order of 20%, assuming the BLM is positioned about 200 cm from the center of the quadrupole.

2.3.4 Longitudinal position dependence

Simulations of point-losses with incident angle of 0.2mrad and energy of 200GeV in the up position were done. The field in quadrupole is 26.6T/m. The position of the loss was shifted ±20 cm from the center of the yoke.

"Position": The position of the maximum relative to the middle of the quadrupole yoke.

Position of losses	bottom of vessel	Position [cm]	Width [cm]	Counts [/e/cm^2]	top of vessel	Position [cm]	Width [cm]	Counts [/e/cm^2]
25 cm		150	229	$3.8 \cdot 10^{-3}$		181	272	$3.7 \cdot 10^{-4}$
12cm		128	233	$4.1 \cdot 10^{-3}$		177	282	$3.0 \cdot 10^{-4}$
0cm		107	195	$6.3 \cdot 10^{-3}$		171	311	$1.7 \cdot 10^{-4}$
-12cm		139	197	$6.5 \cdot 10^{-3}$		193	345	$1.3 \cdot 10^{-4}$
-25cm		179	200	$5.8 \cdot 10^{-3}$		214	382	$9.1 \cdot 10^{-5}$

Table 3: Longitudinal dependencies

Since the quadrupole length is smaller than the length (Width) of the shower distribution outside the vessel, the signal measured downstream is nearly independent of the exact position of the loss. Only losses which occurs not in the yoke will change significant the response of a BLM, but these kinds of losses can not happen without significant more losses in the quadrupole.

2.4 Conclusions from Monte Carlo Calculations

The large length of the shower distribution outside the cryostat makes the calibration of beam loss monitors nearly independent of the exact longitudinal position of the monitor and of the incident angle. A suitable position for a BLM is around 200 cm from the middle of the quadrupole on top of the cryostat. The sensitivity of BLMs can be increased by about a factor 10 at the cost of more complicate mounting, by installing them at the bottom of the cryostat about 180 cm from the middle of the quadrupole.

The energy deposition in 300 mm silicon, in 1 liter of air and the number of charged particles outside the cryostat were found to be linearly dependent on each other:

(Energy dep./ 300 μm silicon) / (Charged particles/cm^2) = 380 ± 40 [KeV/particle] or

(Energy dep./ 1g silicon) / (Charged particles/cm^2) = 5.5 ± 0.6 [MeV/(g/cm^2)/particle]

and

(Energy dep. / 1 liter of air) / (Charged particles / cm^2) = 4.1 ± 0.36 [MeV/liter/particle]

and

(Energy dep. / 1 liter of air) / (Charged particles /cm^2) = 3.2 ± 0.3 [MeV/(g/cm^2)/particle]

The BLM signal depends linearly on the incident electron energy for energies up to 250GeV. Therefore each BLM position has a unique calibration factor which depends only on the energy of the beam at that position. At larger energies in the Linac the non-linearity of the calibration has to be taken into account.

2.5 Energy deposition in the superconductors; quench protection

The electromagnetic shower produced by a beam loss deposits energy in the following superconducting structures, e.g. the quadrupole coil and the cavity. The energy deposition in the coil and cavity for a beam loss in the center of the quadrupole was calculated and is shown in the following table for the hottest point of the structure:

Energy [GeV]	Field [T/m]	Dep. energy in coil [GeV/e/cm^3]	[mJ/e/cm^3]	Dep. energy in cavity [GeV/e/cm^3]	[mJ/e/cm^3]
5	1	0.018	$2.9 \cdot 10^{-9}$	0.24	$3.8 \cdot 10^{-8}$
25	5	0.088	$1.4 \cdot 10^{-8}$	0.64	$1.03 \cdot 10^{-7}$
50	10	0.18	$2.9 \cdot 10^{-8}$	1.01	$1.62 \cdot 10^{-7}$
100	19.8	0.41	$6.6 \cdot 10^{-8}$	1.42	$2.3 \cdot 10^{-7}$
125	24.8	0.58	$9.3 \cdot 10^{-8}$	1.53	$2.5 \cdot 10^{-7}$
150	20	0.70	$1.1 \cdot 10^{-7}$	2.2	$3.5 \cdot 10^{-7}$
200	26.6	0.95	$1.5 \cdot 10^{-7}$	2.7	$4.3 \cdot 10^{-7}$
250	33.3	1.3	$2.1 \cdot 10^{-7}$	3.0	$4.8 \cdot 10^{-7}$
400	53.2	2.2	$3.5 \cdot 10^{-7}$	4.6	$7.4 \cdot 10^{-7}$

Tab. 4: Energy deposition in the superconducting parts at a beam loss

For example, about 10^7 lost electrons can deposit enough energy to quench the quadrupole at 125 GeV, assuming the critical current limit of 1 mJ/cm^3 (worst case).
The beam injection is proposed as train of 0.8ms length with 2820 bunches with bunch spacing 337ns. The repetition frequency will be 5Hz. The losses might be distributed over the whole train, which gives a critical loss rate of 10^7 /0.8 e$^-$/ms or 10^7 / 2820 = 3800 e$^-$/bunch. The critical loss rate will increase by up to a factor 10 at lower quadrupole currents. However, any loss monitor system should detect the minimal critical loss rate reliable.
A cryogenic time constant of 20ms is assumed from experiences from Tevatron and HERA. A BLM system should be much faster than this time constant to prevent the magnets from beam loss induced quenches. A time scale of about 1/10 of a pulse train (~80 μs) seems to be adequate.

beam energy [GeV]	critical energy deposition in coil [mJ/cm^3]	required BLM sensitivity [lost e/bunch]
5	10	1 240 000
100	5	27 000
125	1	3800
400	1	1000

Table 5: Required BLM sensitivity

3 Different Monitor Systems

The calibration of a single beam loss monitor in terms of lost electrons/signal depends on the energy of the lost particle, because the number of shower particles increases with increasing energy. Therefore the calibrations at each location in the LINAC will be different.
The BLMs need to be positioned downstream the quadrupoles within the FWHM of the shower, i.e. 2m. The variation of the maximum of the shower leakage due to different beam energies and loss locations inside the quadrupole is much smaller than the FWHM of the distribution. Therefore the error of the calibration of a beam loss monitor is always less than a factor 2. One has to multiply furthermore a factor 2 to the calibration error due to the shower asymmetry at high quadrupole fields. For the following calculations, the maximum value was always taken.
The shower intensity is about a factor 10 higher at the bottom of the vessel than on top. For the best sensitivity, it is assumed that the monitors are mounted below the cryostat, though the mechanical mounting is more complicated.

3.1 Distributed BLMs

Ion chambers, PIN diodes, Photomultipliers and Scintillation Counters are currently used for beam loss monitor systems in many accelerators (Ref. 4). Scintillation Counters can be made of any required volume, so that it will match to the required sensitivity. They will be fast enough to analyze the losses of each bunch. The main problem will be, that each multiplier needs a stabilized high voltage and that most types of scintillators are sensitive to radiation damage. PIN diodes and Ion chambers have shown very good radiation hardness. Therefore we will discuss in the following three different types of BLMs: Air filled Ion chambers, PIN diodes in counting mode and PIN diodes in current mode readout. The following table summarizes some important properties of the different detector types.

Property	Si-PIN diodes "Counting technique"	Air filled ion chamber	Silicon detector "Current mode"
Dynamic range	$<3\cdot10^3$ because of number of bunches in the pulse train	5nA-10mA ADC range=10^4	5nA-10mA Dynamic range is up to the 10^5. ADC range=10^4
Bunch resolution.	The response to bunch is 0 or 1 count. **No bunch resolution**. For 1/10 sampling of the train dynamic range is $\sim3\cdot10^2$.	Time resolution >1000ns. **No bunch resolution**.	Time resolution ~ 30ns. For 1/10 sampling dynamic range is 10^4 without problems. $\sim10^3$ for bunch resolution
Readout	simple counters	Preamplifier and ADC	Preamplifier and ADC

Table 6: Some detector properties

The sensitivity of each type can be derived from chapter 2.5. The sensitivity is defined by the minimum detectable signal. It is for the counting technique obviously one count, for the ion chamber and for the silicon detector it is limited by the dark current of the detector (about 5 nA). The signal produced in the detector can be calculated by:

- Silicon detector: 3.6eV is needed to create an electron/hole pair in silicon. In a detector of 1 cm^2 area and a width of 300 μm depletion layer one has a deposed energy of E_{dep}=Value [MeV/g/ e^-]·density [g/cm^3]·area [cm^2]·width [cm]=Value·2.33·1·0.03 [MeV/e^-] and therefore $E_{dep}/3.6$ = N number of electron/hole pairs / lost e^-. N multiplied with the required BLM sensitivity gives the critical signal in the detector, which has to be measured at quench level. The minimal detectable signal should be at least a factor ten below. The last column in the table 6 shows the number of lost electrons/bunch which produce a signal just above the noise level of the BLM system.

beam energy [GeV]	critical energy deposition in coil [mJ/cm^3]	required BLM sensitivity [lost e/bunch]	E_{dep} in detector [MeV/e]	critical signal $\cdot 1.6 \cdot 10^{-19}$ [C/bunch]	BLM sensitivity [e/bunch/ 5 nA]
5	10	1 240 000	$3.4\cdot10^{-5}$	$1.2 \cdot 10^7$	1100
100	5	27 000	$1.1\cdot10^{-3}$	$8.4 \cdot 10^6$	35
125	1	3800	$1.2\cdot10^{-3}$	$1.2 \cdot 10^6$	30
400	1	1000	$1.2\cdot10^{-2}$	$3.3 \cdot 10^6$	3

Table 6: Results for silicon detector

- Ion chamber: About 30 eV is needed to create an electron/hole pair in air. ThereforeDep. energy Air / 30 = N is the number of created electron/hole pairs / lost ë. ¯. N multiplied with the required BLM sensitivity gives the critical signal in the detector, which has to be measured at quench level. The minimal detectable signal should be at least a factor ten below. The last column in the table 7 shows the number of lost electrons/bunch which produce a signal just above the noise level of the BLM system.

beam energy [GeV]	critical energy deposition in coil [mJ/cm^3]	required BLM sensitivity [lost e/bunch]	E_{dep} in detector [MeV/e]	critical signal $\cdot 1.6 \cdot 10^{-19}$ [C/bunch]	sensitivity [e/bunch/5 nA]
5	10	1 240 000	$3.2 \cdot 10^{-4}$	$1.3 \cdot 10^{7}$	1000
100	5	27 000	$1.1 \cdot 10^{-2}$	$9.9 \cdot 10^{6}$	29
125	1	3800	$1.2 \cdot 10^{-2}$	$1.5 \cdot 10^{6}$	26
400	1	1000	$1.3 \cdot 10^{-1}$	$4.3 \cdot 10^{6}$	2.4

Table 7: Results for Ion chamber

A minimum critical signal of about $2.1 \cdot 10^{-13}$ C/bunch can be observed in case of the ion chamber and the silicon detector. Assuming an electronic integration time of the bunch spacing, a current of about 600 nA will be measured. This signal can be measured with standard electronics and has still a dynamic range of more than 100. Using longer integration, e.g. for the ion chamber, times can increase the dynamic range due to noise reduction.

- Counting mode: The required BLM sensitivity multiplied with the Counts/e/cm^2 and with the electronic efficiency of such a detector of 30% (Ref. 5) gives the critical signal rate [counts/bunch]. However, the maximum rate can not exceed 1 count / bunch. Therefore the result indicates, that the maximum rate is reached some factors before the quench limit. Assuming an integration time of 1/10 of the pulse train (282 bunches), one might set a critical threshold to about 200 counts within the integration time. This threshold is still some factors below the critical loss rate but offers a dynamic range of 200. The last column in the table 8 shows the number of lost electrons/bunch which produce a signal just above the noise level of the BLM system (e.g. 1 count).

beam energy [GeV]	critical energy deposition in coil [mJ/cm^3]	required BLM sensitivity [lost e/bunch]	Counts [/e/cm^2]	critical signal [Counts/bunch]	sensitivity [e/1 count]
5	10	1 240 000	$8.3 \cdot 10^{-5}$	30	$4.0 \cdot 10^{4}$
100	5	27 000	$2.5 \cdot 10^{-3}$	20	$1.3 \cdot 10^{4}$
125	1	3800	$2.9 \cdot 10^{-3}$	4	950
400	1	1000	$2.7 \cdot 10^{-2}$	9	110

Table 8: Results for Counting mode

4 Conclusion

The three discussed BLM types are all sensitive enough to reliably measure beam losses far below the quench limit. Therefore they might be extremely useful also for beam steering purposes. With the Silicon detector and the ion chamber beam losses of less than 100 electrons at energies above 100 GeV can be resolved, which is about two orders of magnitude below the quench limit. The sensitivity of the simple counting technique is about one order below the quench limit over the energy range of the TESLA Linac. A dynamic range of better than 100

can be achieved with the BLMs. The silicon detector offers a bunch by bunch loss measurement by using a fast preamplifier and fast ADCs. The ion chamber and PIN diode counting mode need longer integration times (1μs and 80 μs, respectively). The advantage of the counting mode is the simple (and therefore more reliable) readout system without the need of ADC converters. Good performance has been achieved with the counting technique at HERA. A disadvantage is that very high losses within one bunch cannot be resolved and that such a system is about one order of magnitude less sensitive to beam losses than the other examined BLM readout methods.
In general, the sensitivity of the BLMs that is calculated for the high-energy beam can be assumed for the magnets at the beam delivery system at TESLA. It provides a sensitive way to detect very small beam losses in that region. Moreover, the calculated sensitivities at other energies can be used for a first guess for the response of BLMs at other locations e.g. undulator transfer lines, damping rings, etc. Detailed Monte Carlo studies with the exact magnet geometry at this locations will be necessary to calculate more precise numbers.
Other BLM systems are still under study: First encouraging results where made at TTF with Cherenkov light detection from fiber optics (Ref. 6), which has the advantage of a fast response and a small number of readout channels.
A system (Compton battery) which is expected not to be sensitive to dark current background (see Appendix 1) will be tested soon in TTF (Ref. 7).
The dose due to radiation from beam losses and dark current (see Appendix 1) inside the TESLA tunnel can be measured by a fiber optic system, too. Preliminary tests in TTF and a general layout for TESLA are described in Ref. 8, 9.

5 References

Ref. 1: R. Brinkmann, G. Materlik, J. Rossbach, A. Wagner (Ed.): Conceptual Design of a 500 GeV e+e- Linear Collider with Integrated X-ray Laser Facility. DESY-97-048 and ECFA- 97-182

Ref. 2: S. Wolf, DESY-MKS, private communication

Ref. 3: Assuming $T_{critical}$ = 7 K at 25 MV/m and spec. heat cap. c_p = 3000 J/K/m^3 for Nb. Numbers from D. Reschke, DESY-MHF-SL; private communication.

Ref 4: K. Wittenburg , Beam Loss Detection ,Proc. 1st European Workshop on Beam Diagnostics and Instrumentation for Particle Accelerators, Montreux, Switzerland, 3-5.5.1993, CERN PS/93-35 (BD)

Ref. 5: K. Wittenburg, THE PIN-DIODE BEAM LOSS MONITOR SYSTEM AT HERA. DESY-HERA-00-03, Jun 2000. 15pp.

Ref. 6: E. Janata et al.: Radiation detection by Cherenkov emission in fiber optical cables in TTF, DESY TESLA 2000-27

Ref. 7: P.J.T. Bruinsma, J.B. Spelt, TESLA report in preparation., See also: A FAST BEAM PROTECTION SYSTEM.(TALK). By A. Maaskant & P.J.T. Bruinsma, IEEE Trans. Nucl. Sci. 28 (1981) 2367-236.

Ref. 8: H. Henschel et al.; DESY TESLA 2000-25 "Preliminary Trails with Optical Fiber Dosimeter at TTF"

Ref. 9: H. Henschel et al.; DESY TESLA 2000-26 "Fiber Optic Radiation Sensing Systems for TESLA"

Appendix: Field emission electrons from the accelerating module

High gradient superconducting cavities will be used in TESLA. At high gradients electrons can be produced due to field emission (Ref. A1). The detailed structure of this dark current is not fully understood yet. In Ref. A2 the intensity, spectrum and spatial distribution of dark current are presented. The current is uniformly distributed over the beam pipe at the end of an accelerating module in front of the quadrupole. The energy of the electrons can exceed several hundred MeV while the main of the spectrum is in the range between 20 - 200MeV. The initial conditions in the Monte Carlo studies were: A uniform spatial distribution of electrons with angles = 0 and a uniform energy distribution in the range 20-200MeV at the upstream edge of a quadrupole with a field length of 51.6cm. Two cases are considered: strong (26.6T/m) and weak (1 T/m) quadrupole fields corresponding to 200GeV beam and 5GeV beam, respectively. The figures A1 a-f show a strong dependence of the created shower on the gradient and on the focussing direction of the quadrupole. A general rule cannot be given for these kind of events. However, one can estimate the response of the BLMs using the following numbers:
The counting rate in the bottom zone is about $2 \cdot 10^{-6}$ counts/e/cm^2 at the maximum for a X focusing quadrupole field 1T/m (Fig. A2 a). The energy deposition at the maximum is $1.2 \cdot 10^{-5}$ MeV/g/e ($E_{dep} = 8.4 \cdot 10^{-7}$ MeV/e) in a 300 µm Silicon layer or $8.2 \cdot 10^{-6}$ MeV/liter/e in 1 liter air. In Ref A2 a dark current at the quadrupoles is calculated to be about 2 µA at an accelerating gradient of 22 - 25 MV/m which is equivalent to 10^{10} e/800 µs. This results in signals of (1 pulse = 800 µs):

- For the counting mode (1 cm^2 active area):
  $(2 \cdot 10^{-6}$ counts/e/cm$^2) \cdot (10^{10}$ e/pulse) = $\underline{2 \cdot 10^4$ counts/pulse}
- For silicon detector (1 cm^2 active area, 300 µm depletion layer)
  $(8.4 \cdot 10^{-7}$ MeV/e) / (3.6 eV/e-hole) $\cdot (10^{10}$ e/pulse) = $\underline{2 \cdot 10^9 (\cdot 1.6 \cdot 10^{-19})}$ C/pulse
- For ionization chamber (1 litre air)
  $(8.2 \cdot 10^{-6}$ MeV/liter/e) / (30 eV/e-hole) $\cdot (10^{10}$ e/pulse) = $\underline{2.8 \cdot 10^9 (\cdot 1.6 \cdot 10^{-19})}$ C/pulse

These values are of the same order of the critical signals (see chap. 3.1).
Note that these dark current electrons are modulated with 1.3 GHz and not with the bunches. Therefore gating with the bunches will help to reduce these additional signals without reducing the signals from real beam losses (by a factor 1.3 GHz · 337 ns = 438) . But gating will work only with the fast silicon detectors and not with the slow ionization chambers. Another way to select the dark current events from the beam losses might be to measure the dark current signal individually at each BLM without beam and subtract the value from the signal with beam. But the uncertainty of this procedure might be too large if the dark current signal is of the same order, or even larger, than the beam loss signal. A solution can be to install an other type of beam loss monitor system, which is expected to be not sensitive to the dark current (Ref. 7).

Appendix: Quench issue

The energy deposition in the quadrupole coil due to the dark current was also calculated:
The deposited energy in the hottest point of the quadrupole coil would be $6 \cdot 10^{-4}$ GeV/e/cm^3 (= $1 \cdot 10^{-10}$ mJ/e/cm^3) in the worst case of a strong magnetic field. Therefore 10^{10} e/pulse (2µA) at the beginning of the quadrupole would deposit 1mJ/cm^3 in the coil. This is close to the critical energy deposition in the quadrupole and has to be added to the real beam losses. Therefore it is important to reduce the dark current of an accelerating module by some orders of magnitude. The latest improved cavities studied at DESY show gradients of more than 30 MV/m with a Q-value of better than $5 \cdot 10^9$, indicating that the dark current produced in these cavities is very small at design gradients.

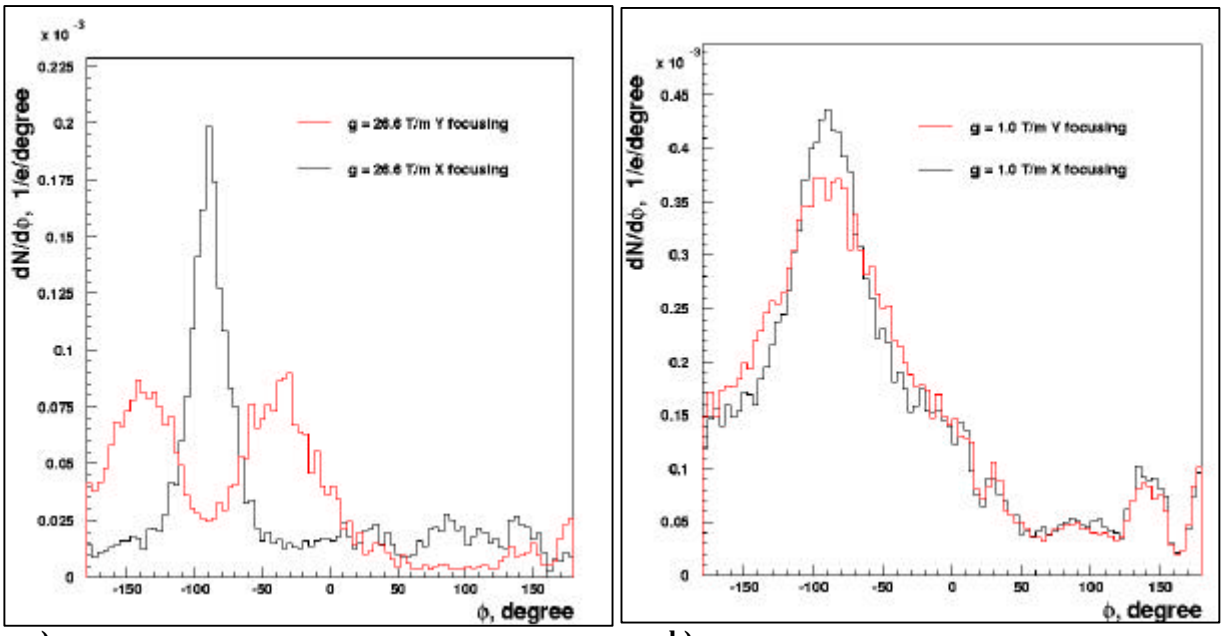

a) **b)**

Fig. A1: Azimuthal angle distribution of charged particles on the surface of vacuum vessel. The field emission electrons are uniformly distributed in energy (20-200 MeV) and space (beam pipe). a) Field gradient 26.6T/m for Y focusing and defocusing quadrupoles, b) quadrupole field gradient 1 T/m.

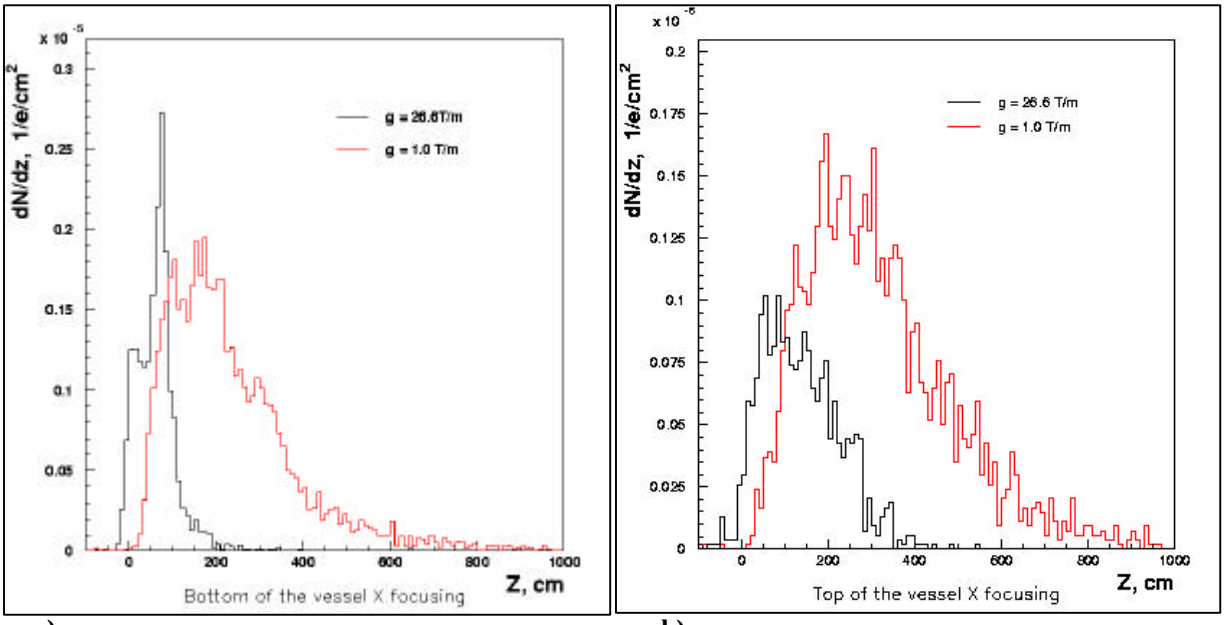

a) **b)**

Fig. A2: X focusing quadrupole. Z distribution on the surface of the cryostat for different field gradients. a) Bottom zone of the vessel. b) top zone of the vessel.

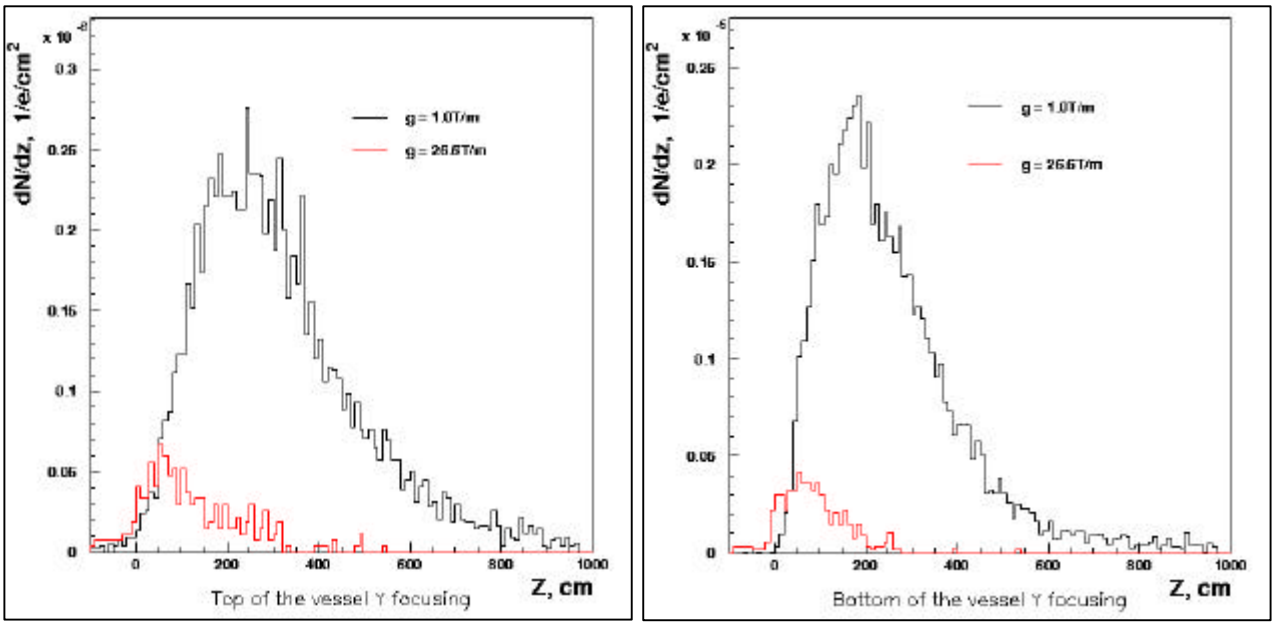

a) **b)**

Fig. A3: Y focusing quadrupole. Z distribution on the surface of the cryostat for different field gradients. a) Bottom zone of the vessel. b) top zone of the vessel.

References Appendix

Ref. A1: B. Bonin, Field emission in RF cavities, CAS superconductivity in particle accelerators, 17-24 May 1995, Rissen, Hamburg, Germany, CERN 96-03, pp. 221-228

Ref. A2: Ch Stolzenburg: Untersuchung zur Entstehung von Dunkelstrom in supraleitenden Beschleunigungsstrukturen, Thesis, University Hamburg 1996